Anomalous X-ray Reflectivity Characterization of Ion Distribution at Biomimetic Membranes

David Vaknin,[1] Peter Krüger,[2] and Mathias Lösche[2,*]
[1] *Ames Laboratory and Department of Physics and Astronomy, Iowa State University, Ames, Iowa 50011, U.S.A.*
[2] *Institute of Experimental Physics I, Leipzig University, Linnéstr. 5, D-04103 Leipzig, Germany*
[*] *also at the Department of Chemical and Biomolecular Engineering, The Johns Hopkins University, Baltimore, Maryland 21218, U.S.A.*
(Dated: January 14, 2003)

A novel approach based on anomalous X-ray reflectivity measurements provides detailed information on ion binding to biomembrane surfaces. Using a high intensity monochromatic beam tuned to various X-ray energies at Argonne National Lab's Advanced Photon Source and utilizing a newly commissioned X-ray liquid surfaces reflectometer, measurements at and away from ion absorption edges allow determination of the distribution of these ions as they accumulate near lipid membranes. As a model, the interaction of dissolved Ba^{2+} ions with $DMPA^-$ (1,2-dimyristoyl-*sn*-glycero-3-phosphatidic acid) monolayers at the aqueous surface as studied. We find an unexpectedly large concentration of barium at the interface, ≈ 1.5 per $DMPA^-$, forming a Stern layer of bound ions and a cloud of less densely bound ions near the lipid headgroups. This result can only be understood if one assumes that bound cations are partially speciated, *e.g.*, as $BaOH^+$.

PACS numbers: 87.16.Dg, 87.14.Cc, 05.65.1b, 87.64.Bx

Ions at cell membrane surfaces affect the function and conformation of nearby molecules and play thus an important role in inter- and intracellular transport, as well as in recognition processes [1, 2]. Moreover, charge patterns at membrane surfaces may direct crystal growth in biomimetic mineralization processes [3, 4]. As model systems for biomimetic interfaces, Langmuir monolayers (LM) have been widely employed [3–7]. LMs consist of molecular lipid surface layers into which proteins or other molecules of biological or physiological relevance may be incorporated. Such a "bottom up" approach for biomineralization has already shed light on some of the involved mechanisms. For example, the charge distribution which eventually directs the morphology of product crystals can be controlled by the choice of functional headgroups and their density, as well as the subphase pH, ionic strength, and temperature [3–6]. X-ray reflectivity (XR) and diffraction at grazing angles of incidence (GIXD) are well suited for structural characterization of interfaces on the molecular length scale [8]. GIXD is a superior characterization technique for the determination of periodic in-plane arrangements of molecules; however, this requires that the layer be crystalline. This is in biological systems only rarely the case (*e.g.*, in the purple membrane of halobacteria [9]) as almost all biological membrane systems are characterized by – and require for their proper function – a large degree of structural and dynamic disorder. X-ray (or neutron) reflection techniques [8] are well suited to determine the scattering length density distributions normal to the interface due to organic layers of ordered *or disordered* constituents. From such one-dimensional profiles, information on the (averaged) in-plane distribution of submolecular fragments may be inferred by means of slab models [10] or volume-restricted chemical models [11].

Several X-ray fluorescence methods probe adsorbed ions at solid and liquid interfaces. In the near-total-external fluorescence (NTEF) technique [12], the K_α fluorescence from an illuminated sample is monitored as a function of the incident angle on the surface. Similarly, the x-ray standing wave (XSW) technique [13] can probe the location of an ionic layer with respect to the substrate. It requires, however, that the ionic layer is exterior to the substrate surface [13]. Both techniques do not provide a global structural picture of an absorbed layer with respect to other constituents of the film.

Here, we exploit the anomalous scattering of X-rays by collecting reflectivity data at different energies, at and away from the absorption edge of the probed ions. With this technique, the effective electron density (ED) profile of the surface film at each energy is determined, and from their differences the contribution of the adsorbed ions is extracted. The advantage of this approach is that it determines the location and distribution *specifically* of those ions whose absorption edge is being probed – potentially even against a background of co-bound ions if the aqueous phase near the membrane has a complex composition. In addition, submolecular details of membrane organization can be revealed [14]. Experimentally, this approach is similar to the method developed by Sanyal et al. [15] for model-independent reconstruction of ED profiles of thin films on Ge substrates. Conceptually, it is also similar to contrast variation in neutron scattering that is capable of highlighting specific, isotopically varied sections within a sample [10]. In this paper, we describe the application of this technique for a characterization of the Stern layer that forms at an anionic LM on highly concentrated $BaCl_2$ solutions. We observe that barium binds in quantities which surpass by far the stochiometric ratio between the lipidic anion and the subphase-borne

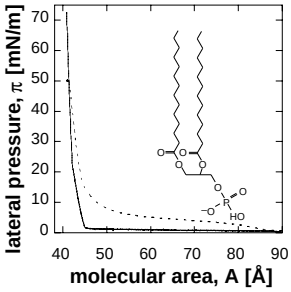

FIG. 1: Chemical structure of DMPA and Langmuir isotherms on H_2O (dashed) and 10 mM $BaCl_2$ (solid line)

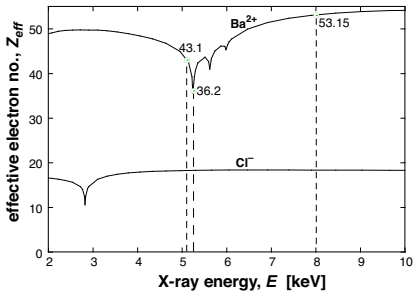

FIG. 2: Effective number of free electrons (Z_{eff}, as discussed in the text) of the ions used in this study [22]. Z_{eff} values for the atomic constituents of DMPA or water do not vary in the energy range shown.

dications. While such an overcompensation has earlier been postulated from conventional (fixed-energy) X-ray reflection experiments [14] using *indirect* arguments that determined a lower limit of the barium concentration at the interface, the novel approach enables an unambiguous quantification of the ions within the constraints of the used model. – In addition, the organization of the lipid headgroups is revealed in submolecular detail.

DMPA (1,2-dimyristoyl-*sn*-glycero-3-phosphatidic acid, Avanti Polar Lipids, Fig. 1) monolayers were spread from $CHCl_3$ on concentrated (10 mM) aqueous $BaCl_2$ (Sigma, purity: 99+%) solutions prepared from ultrapure water (NANOpure, Barnstead, Dubuque, IA) in an encapsulated Teflon Langmuir trough kept under He atmosphere at T = 18^{o}C. Lateral pressure versus molecular area (π vs. A) isotherms of DMPA (Fig. 1) on pure water and on ionic solutions were consistent with published data [14]. A newly commissioned liquid surface diffractometer at the Advanced Photon Source (APS), beamline 6-ID-B, was employed to investigate the structure of the LMs. The highly monochromatic beam (energy resolution, $\Delta E \approx 1$ eV) selected by a downstream Si double crystal monochromator is deflected onto the liquid surface at a desired angle of incidence by another monochromator (Ge(111)) located at the diffractometer [16]. Prior to the measurements, the absolute scale o the X-ray energy was calibrated with 6 different absorption edges to better than $\pm$ 2 eV. – Modern synchrotron sources, such as the APS, permit the determination of X-ray reflectivities of aqueous surfaces out to a momentum transfer, Q_z, that exceeds 0.8 Å^{-1} [14] (where z is the direction normal to the interface). ED profiles across LM's are often refined using slab models to fit the measured reflectivity by non-linear least-squares methods. In this approach, the reflectivity at Q_z is calculated by

$$R(Q_z) = R_0(Q_z)e^{-(Q_z\sigma)^2} \quad (1)$$

where $R_0(Q_z)$ is the reflectivity due to an ED profile composed by step functions, calculated by the recursive dynamical method [17, 18], and σ is an effective surface roughness, accounting for the smearing of the interfaces due to thermal capillary waves, as well as surface inhomogeneities [8, 19]. The variable parameters used to construct the ED across the interface, $\rho(z)$, include the thicknesses of the slabs (d_i) and their corresponding electron densities (ρ_i), as well as σ [20]. Alternatively, high-resolution models have recently been developed that describe the ED profiles in terms of volume-restricted [21] sums of distribution functions of submolecular fragments ('VRDF model') [11].

At X-ray energies E significantly higher than the absorption edges of any constituents in the sample, the electrons are practically free. In the general case, the reflectivity is determined by the refractive index along z,

$$n(z) = 1 - (\delta + i\beta) = 1 - r_0\rho(z)\lambda^2/2\pi - i\mu\lambda/4\pi \quad (2)$$

where r_0 is the classical electron radius, λ is the X-ray wavelength and μ is the linear absorption coefficient of the material. In more detail,

$$\delta(z)+i\beta(z) = \frac{r_0}{2\pi}(\frac{hc}{E})^2 \sum_j N_j(z)Z_j[f_j'(E)+if_j''(E)] \quad (3)$$

where N_j the number density of an atomic constituent of type j with Z_j electrons. To calculate the reflectivity near an absorption edge, we introduce the effective number of Thomson scatterers, $Z_{j,eff}(E) \equiv Z_j f_j'(E)$ (see Fig. 2), and apply the standard techniques for calculating reflectivity in the high-energy limit.

Figure 3A shows normalized reflectivities from a DMPA LM (π = 30 mN/m) on 10 mM $BaCl_2$, measured at $E = 5.247$ keV (Ba L_{III} absorption edge), and $E = 5.1$ and 8.0 keV (off-edge) as indicated. In qualitative terms, all three reflectivities exhibit sharp minima at $Q_z \approx 0.21$ Å^{-1}, and are characteristic of highly organized LMs, as previously shown [14]. However, the reflectivity taken at the Ba absorption edge has a sharper and deeper minimum that is shifted to slightly higher Q_z due to the increased absorption. Also, the overall reflectivity for the edge energy photons is smaller than for those off-edge. This indicates a lower effective ED at 5.247 keV compared to those away from the absorption edge [23].

We started with a two-slab model to obtain a quantitative data interpretation. The 'acyl chain' slab ED, the d_i and σ were constrained to be identical for the

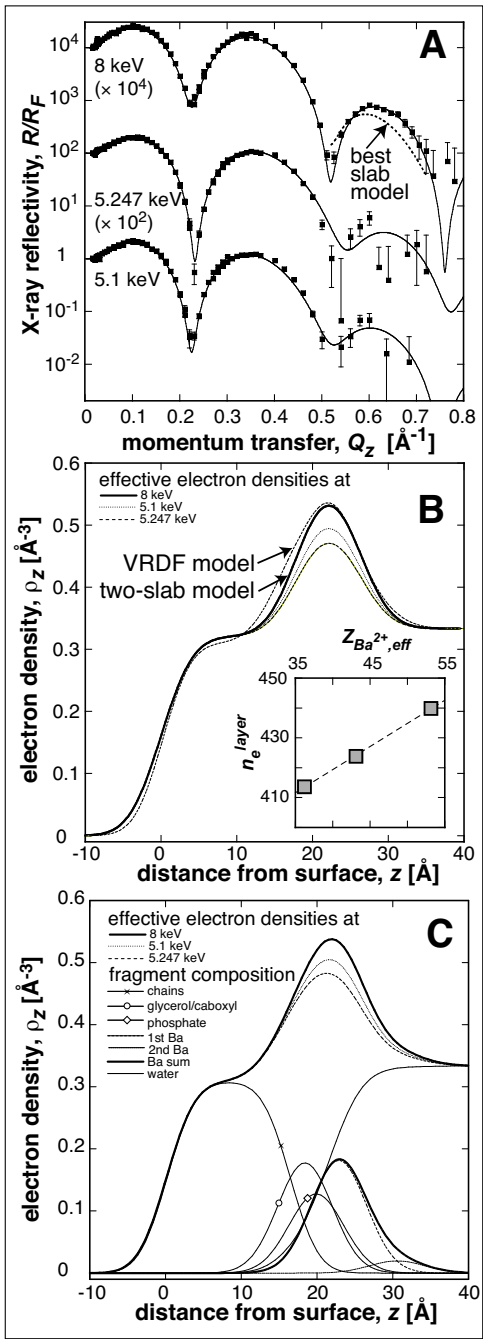

FIG. 3: (A) Fresnel-normalized X-ray reflectivities, R/R_F, of DMPA LMs at $\pi = 30$ mN/m on 10 mM $BaCl_2$ solution at three different X-ray energies. The continuous lines derive from the VRDF model shown in panel (C). (B) Best-fit two-slab ED profile as seen with 8 keV radiation. Corresponding profiles for lower X-ray energies are indicated as dotted lines. The dashed line shows the VRDF profile of panel (C) for comparison. Inset: Apparent number of electrons in the surface layer per area, $A = 41.5$ Å^2, occupied by one DMPA molecule *vs.* the effective number of Thomson scatterers of Ba^{2+}, as E is varied. (C) Best-fit VRDF ED profile at $E = 8$ keV from a simultaneous refinement of 3 data sets. The contributions of submolecular DMPA fragments, ions and water to the overall ED profile are also shown. The corresponding ED profiles for the lower X-ray energies are indicated as dotted lines.

description of all data sets; the EDs of the 'headgroup' slab at the three X-ray energies and its absorption at $E = 5.247$ keV were also treated as independent parameters (*i.e.*, 8 free parameters were refined to describe 3 reflectivity curves simultaneously). Absorptions of the 'acyl chain' and 'headgroup' slabs off-edge are insignificant and were set to zero. Figure 3B shows the resulting ED profiles. It is evident that the effective ED in the headgroup region is lowest at the Ba edge (5.247 keV), as expected. The overall $\chi^2 \approx 8.4$ is reasonable. However, systematic deviations between the model and the data in the high-Q_z regime of the 8.0 keV data set were observed (dotted line below upper trace in Fig. 3A). This is consistent with earlier observations [14] that slab-models describe high-resolution X-ray reflectivity data of LMs particularly poorly in the Q_z regime beyond the second interference minimum [24]. – The number of bariums per lipid, $N_{Ba} \approx 1.5$, is determined from the difference in the apparent electron densities of the lipid headgroups and may independently be derived from a plot of n_e^{layer}, the apparent number of electrons in the surface layer within the area occupied by one DMPA, $A = 41.5$ Å^2, against $Z_{Ba^{2+},eff}(E)$ (c.f. inset in Fig. 3B). The linear correlation suggests that differences in the results for the various X-ray energies are *entirely* due to the anomalous index variations; its slope reveals directly – and independent of any chemical interpretation – $N_{Ba} = 1.55 \pm 0.2$; an extrapolation to $Z_{Ba^{2+},eff} = 0$ quantifies the number of electrons, $n_e^{layer,0} \approx 357$, contained in the surface layer within A, as it would appear without the contribution of the bound Ba^{2+} cations.

A more detailed, chemical interpretation is obtained in the VRDF approach [11]. As in the two-slab model, an extraordinarily high electron density in the surface area suggests that more than the stochiometric ratio – 0.5 Ba^{2+}/$DMPA^-$ – of Ba is bound to the LM. This implies that the surface composition is not limited to $DMPA^-$ and Ba^{2+}. Instead, Cl^- [14] or – more likely – OH^-, *e.g.* in the form of $BaOH^+$ [25], may compensate the high cationic charge density at the interface partially [26]. We have thus tested VRDF models in which either both Ba^{2+} and Cl^- were located near the interface or in which Ba^{2+} was the only bound ion species (the ED of OH^- is indistinguishable from that of H_2O). In both cases, the DMPA was parsed into its acyl chains (fragment 1), the carbonyl/glycerol backbone (fragment 2), and the phosphate (fragment 3) [11]. These models were required to describe the experimental data taken at the different X-ray energies simultaneously (with 8 adjustable parameters for the model that includes both Ba^{2+} and Cl^- ions [27]).

Any of the VRDF approaches predicts the experimental data significantly better than the slab model does. A close inspection of the best-fit ED profiles of the competing models, Figs. 3B and C, shows that the ED distribution in the headgroup region is pronouncedly asymmetric in the VRDF case, a feature which the slab model cannot reproduce. Also, fits become progressively bet-

ter ($\chi^2 \approx 4.0$ as compared to ≈ 6.3) if the VRDF model contains an ionic ED contribution further than 5 Å below the phosphate position, either in a population of weakly bound Cl^- anions ($\chi^2 \approx 4.4$) or in a *second* population of Ba^{2+} cations ($\chi^2 \approx 4.0$) with the implication that speciated OH^- leads to charge compensation. This model (*c.f.* Fig. 3C), which describes the experimental data best, predicts for the LM at $\pi = 30$ mN/m that the average chain tilt is 12 deg from the surface normal. The PO_4^- is located 3.5 Å underneath the acyl carbonyls. About 12 H_2O molecules hydrate the complexed lipid headgroup. A large amount of $BaOH^+$ or $Ba(OH)_2$, with a total of ≈ 1.3 Ba per headgroup, is located at an average vertical distance of 3 Å below the PO_4^- where it forms a firmly bound Stern layer. More Ba^{2+} ($\approx 10\%$ of the total Ba at the interface) is located at the headgroup periphery, centered at a position ≈ 10 Å from the phosphate. The location and density of this population suggests it represents a cloud of counter-charges accumulated near the interface, *i.e.*, the tail of the diffuse Debye-Hückel layer. Irrespective of the details of Ba organization at the lipid headgroup, this large total amount of bound Ba is consistently inferred from the anomalous scattering data, independent of the model used. – A systematic study of cation binding to acidic monolayers at low concentrations aimed at a more complete description of the molecular details of ion binding is on its way [28].

The location and density of barium at an anionic LM were examined in this work. Anomalous X-ray scattering showed directly and independently of the model used for data analysis that much more than the stochiometric amount of cations are bound at the interface. To account for charge compensation, it has been suggested that Cl^- anions are incorporated into the DMPA headgroup [14]. However, the anomalous reflectivity approach presented here enables determination of *ion-specific* contributions and yields an even larger barium concentration at the LM. The ion distribution appears to be highly asymmetric and may encompass a firmly bound Stern layer – comprising $BaOH^+$ – as well as a diffuse cloud of Ba^{2+} which represents the tail of the Debye-Hückel layer. The technique we have developed should bear great potential for detailed investigations of the electrostatics of ion binding to surfaces and for a molecular comprehension of biomineralization processes [6].

Acknowledgments

We thank M. Harper for help with diffractometer design and construction and D. S. Robinson for technical help and discussions. The MUCAT sector at APS is supported by the U.S. Department of Energy, Basic Energy Sciences, Office of Science, through Ames Laboratory under contract no. W-7405-Eng-82. Use of the APS was supported by the U.S. DoE, BES, OoS, under contract no. W-31-109-Eng-38. Financial support from the Volkswagen Foundation (grant no. I/77709) and the Fonds der Chemischen Industrie are gratefully acknowledged.

[1] G. Cevc, *Biochim. Biophys. Acta* **1031**, 311 (1990).
[2] J.-F. Tocanne and J. Teissie, *Biochim. Biophys. Acta* **1031**, 111 (1990).
[3] E. M. Landau, et al., *J. Am. Chem. Soc.* **111**, 1436 (1989).
[4] S. P. Weinbach, et al., *J. Am. Chem. Soc.* **115**, 11110 (1993).
[5] B. R. Heywood and S. Mann, *Adv. Mater.* **6**, 9 (1994).
[6] M. J. Lochhead, et al., *J. Phys. Chem B* **101**, 10821 (1997).
[7] F. Leveiller, et al., *Langmuir* **10**, 819 (1994).
[8] J. Als-Nielsen and K. Kjaer, *Proc. NATO ASI Ser. B* **211**, 113 (1989).
[9] J. K. Lanyi, *Nature* **375**, 461 (1995).
[10] D. Vaknin, et al., *Biophys. J.* **60**, 1545 (1991).
[11] M. Schalke, et al., *Biochim. Biophys. Acta* **1464**, 113 (2000).
[12] J. M. Bloch, et al., *Phys. Rev. Lett.* **54**, 1039 (1985).
[13] M. J. Bedzyk, et al., *Science* **248**, 52 (1990).
[14] M. Schalke and M. Lösche, *Adv. Colloid Interf. Sci.* **88**, 243 (2000).
[15] M. K. Sanyal, et al., *Europhys. Lett.* **21**, 691 (1993).
[16] J. Als-Nielsen and P. S. Pershan, *Nucl. Inst. Meth.* **208**, 545 (1983).
[17] M. Born and E. Wolf, *Principles of Optics*. MacMillan, New York (1959).
[18] L. G. Parratt, *Phys. Rev.* **59**, 359 (1954).
[19] D. Vaknin, in *Methods in Materials Research*, ed., E. N. Kaufmann, et al., p. 10d.2.1 (Wiley, New York, 2001).
[20] The number of slabs which is used to fit the data is the minimum necessary in the sense that an additional slab does not further improve the quality of the fit significantly.
[21] R. S. Armen, O. D. Uitto, and S. E. Feller, *Biophys. J.* **75**, 734 (1998).
[22] C. T. Chantler, *J. Phys. Chem. Ref. Data* **24**, 71 (1995).
[23] J. Lekner, *Theory of Reflection of Elementary and Particle Waves*, (Martinus Nijhoff Publishers, Boston (1987).
[24] Because of a smaller X-ray intensity at 5.1 and 5.247 keV, data scatter in the high-Q_z regime there is too large to afford a distinction of the alternate models.
[25] M. Beyer, E. R. Williams, and V. E. Bondybey, *J. Am. Chem. Soc.* **121**, 1565 (1999).
[26] Similarly, Als-Nielsen and coworkers [7] have observed a situation in which $CdOH^+$ was shown to be firmly bound to arachidic acid monolayers from $CdCl_2$ solutions.
[27] Fragment 2 was located in a fixed relative position underneath fragment 1. Fragments 2 and 3 as well as the ions were distributed with the same thermal broadening added upon the conformal surface roughness deriving from capillary waves. The amount of Cl^- bound to the LM is deduced from the assumption of charge compensation at the surface [11].
[28] J. Pittler, et al., (to be published).

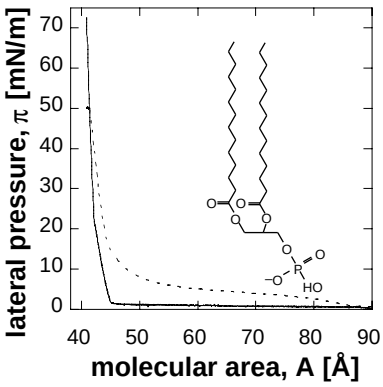
lateral pressure, π [mN/m]
70
60
50
40
30
20
10
0
40
50
60
70
80
90
molecular area, A [Å]
O
O
O
O
O
O
O
P
O
–O
HO

Figure 1

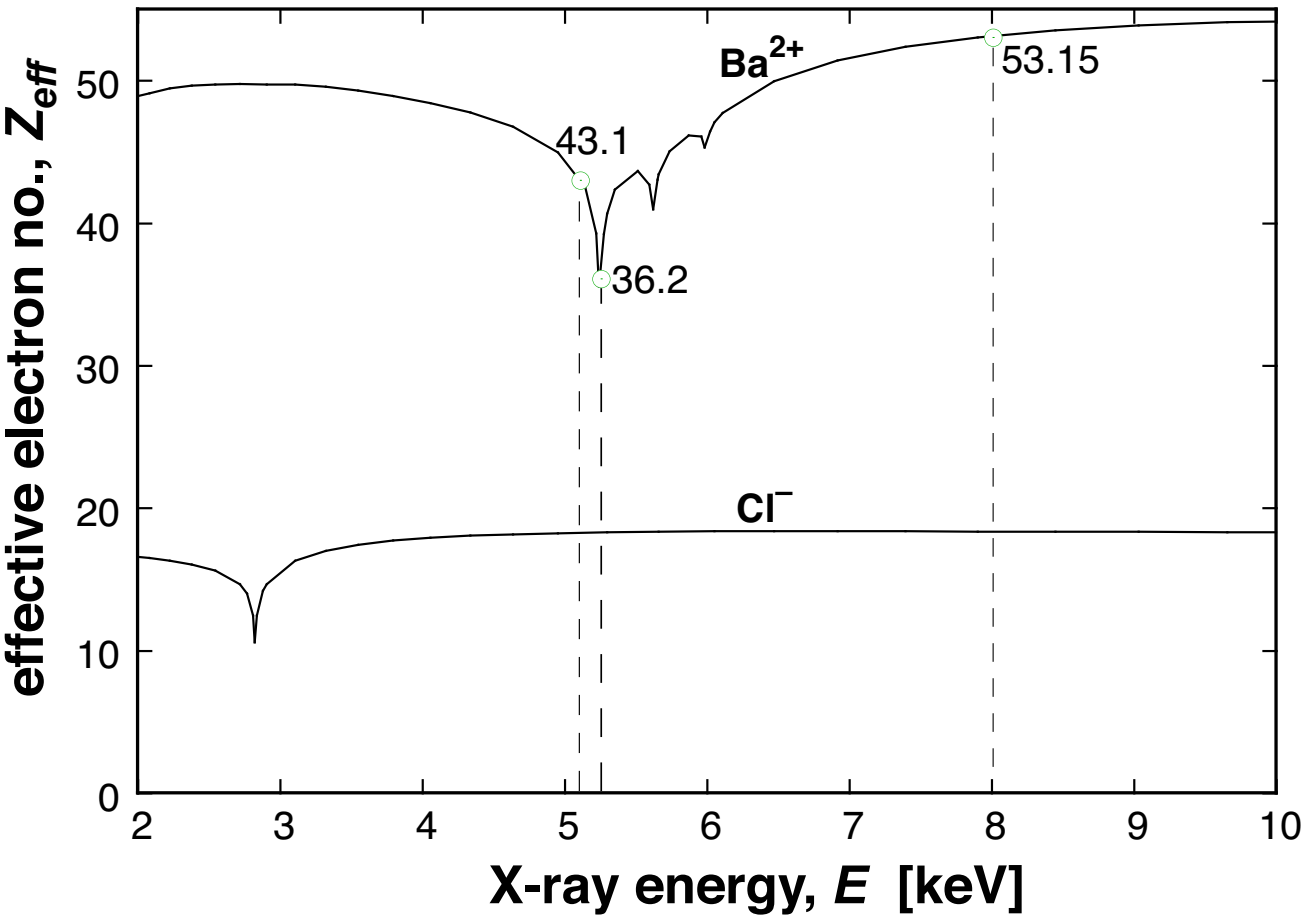
effective electron no., Z_{eff}
X-ray energy, E [keV]
Ba^{2+}
Cl^-
43.1
36.2
53.15
0
10
20
30
40
50
2
3
4
5
6
7
8
9
10

Figure 1

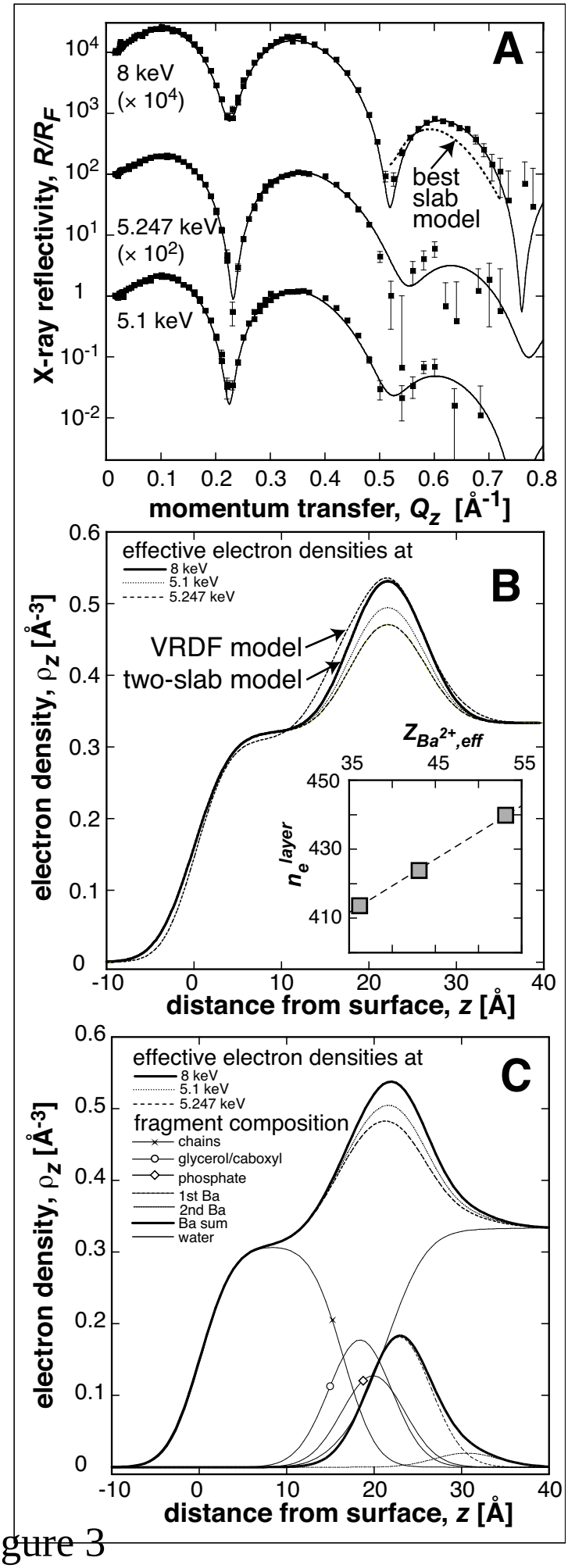
A
8 keV
(× 10^4)
5.247 keV
(× 10^2)
5.1 keV
best
slab
model
X-ray reflectivity, R/R_F
momentum transfer, Q_z [Å^-1]
B
effective electron densities at
8 keV
5.1 keV
5.247 keV
VRDF model
two-slab model
Z_Ba2+,eff
n_e^layer
electron density, ρ_z [Å^-3]
distance from surface, z [Å]
C
effective electron densities at
8 keV
5.1 keV
5.247 keV
fragment composition
chains
glycerol/caboxyl
phosphate
1st Ba
2nd Ba
Ba sum
water
electron density, ρ_z [Å^-3]
distance from surface, z [Å]

Figure 3